Control
and Cybernetics
VOL. 14 (1985) No. 1—3

Free boundaries in induction heating *)

by

A. BOSSAVIT

Direction des Etudes et Recherches
Electricité de France
1 Avenue du Général de Gaulle
92141 Clamart, France

This paper reports a series of numerical experiments on the simulation of inductive heating of steel slabs, a phenomenon which exhibits interesting free boundaries, and raises some theoretical questions. More, the very presence of moving boundaries is connected with the efficiency of the heating, and this leads to control problems which were the starting point of these studies. Results were put in the form of a computer-generated film (first shown during the Maubuisson conference on "Free boundaries, Applications and Theory" (1)). Here we shall describe the problem and the relevant numerical methods, and comment on the contents of the film, with the help of selected sequences of frames.

In inductive heating, the steel workpiece behaves like the secondary winding of a transformer: a primary inductor generates a magnetic field, whose time-variations induce electromotive forces in the workpiece. These give birth to so-called "eddy-currents", which heat up the steel by Joule effect.

At the Curie point (760°C), steel undergoes a phase transition, with associated rapid changes in such characteristics as resistivity and magnetic behaviour. Due to the latent heat of the transition, the heat diffusion problem is Stefan-like. (By this, we mean the enthalpy curve shows a rapid increase in the vicinity of the Curie point, and when this rapid change is assimilated, for the purpose of modelling, to a discontinuous jump, one gets the classical Stefan problem). In order to get the right-hand side of this heat equation, one should determine the induced magnetic field. This problem is again Stefan-like, as we shall see, in regions whose temperature is below the Curie point. So there are in this situation two coupled Stefan-like problems.

In view of applications to induction heating, and more precisely to the optimal control of the heating process in factory conditions, it was felt necessary to have detailed information about the behaviour of the solution to this coupled problem. In particular, new insight on the phenomenon known as "skin-effect" was necessary. Skin-effect is the accumulation of currents below the surface of the work-piece, in contrast to the behaviour of direct currents, which tend to occupy all the conductive material. Its characteristics are very different under and above the Curie point. Much can be learned on this through analytical investigation (Part 1), but only numerical simulation (Part 2) was able to display the transition from one regime to the other, thus giving the full picture.

*) (Comments on a Computer-Generated Movie on the Numerical Simulation of Two Coupled Stefan Problems)

1. Modelling, and analytical study of the model

1.1. The Equations

1.1.1. A one-dimensional situation

Fig. 1 explains the concept of induction heating as applied to so called "flat products" like steel slabs. Typical dimensions of a slab are (in meters) $0.2 \times 1. \times 5.$ An aluminum conductor (of generous cross section, as it should carry about 10 to 20 kiloAmpère) is wrapped around the slab, along its longer side, thus forming two current sheets which generate an alternating field of about 10^5 A/m in the airgap. The frequency is the main one (50 Hz in France, and in our simulations). Eddy-currents (which are roughly parallel

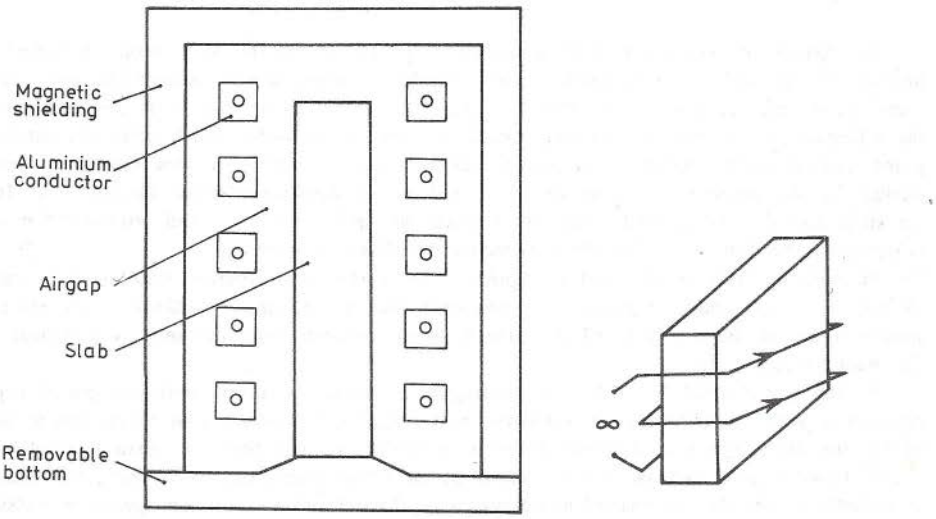

Fig. 1.

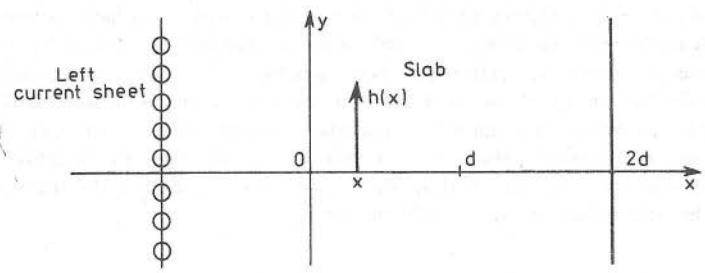

Fig. 2

to the z-axis) appear in the slab and heat it by Joule dissipation. The power thus injected is of the order of a megawatt by square meter of slab surface. This requires a sophisticated alimentation system (power thyristors), which allows to control both power input and frequency, and even the shape of the wave if necessary.

Even at such levels of power, the full heating cycle (which, for obvious economic reasons, should be as short as possible, though avoiding excessive thermal stresses), may require a full hour. Ideally, one should achieve an even temperature profile, at $1200 \pm 10°C$, before proceeding to the forming phase of the elaboration of steel. One may wait for heat diffusion to take place. But one could hasten the process if the Joule power was evenly distributed in the piece. Skin effect opposes that. So skin effect should be, in some way, controlled. This is feasible, since two control parameters (overall input power and frequency) are available, but first depends on a precise knowledge of the dependence of skin-effect on the temperature of the slab. For as temperature goes up, electrical properties of steel change very much, and this determines skin-effect in noneasily predictable ways.

Obviously, the situation calls for one-dimensional modelling. It will be assumed that all phenomena are invariant in y and z (Fig. 1). Due to symmetry, only the left half of the slab will be considered. Abscissas 0 and d respectively (Fig. 2) correspond to the left side and to the middle plane.

1.1.2. "Electric" part of the model

The magnetic field (which is roughly parallel to $0y$ in Fig. 1) is characterized by its magnitude in the y direction. The eddycurrents density is

$$j(x, t) = \partial/\partial x \, h(x, t) \tag{1}$$

(currents are parallel to the z axis). Notice that j is, just like the inducting current, odd with respect to origin d ($j(x, t) = -j(2d - x, t)$), thus h is even, so we have as natural boundary condition

$$\partial h/\partial x \, (d, t) = 0. \tag{2}$$

At $x = 0$, on the other hand,

$$h(0, t) = H \sin \omega t, \tag{3}$$

where H is the peak value of the magnetic field in the airgap (a controllable parameter, and so is the pulsation ω). As for h inside $]0, d[$, we have

$$\frac{\partial}{\partial t} \beta_\theta (h(x, t)) \frac{\partial}{\partial x} \left(\varrho_\theta \frac{\partial h}{\partial x} \right) = 0, \, 0 < x < d. \tag{4}$$

Function β_θ is the "magnetization characteristics" of steel. A widely accepted form for β is the so-called "Fröhlich's model":

$$\beta_\theta(s) = \left(\mu_0 + \frac{b_\theta}{h_\theta + |s|}\right) s. \tag{5}$$

Here, $\mu_0 = 4\pi\, 10^{-7}$ (in S.I. units), b_θ and h_θ are constants which respect to s. Figures 3 and 4 show how they depend on θ. (Numerical values come from (3). Remark that magnetic hysteresis is neglected in the modelling. This is correct, since this phenomenon contributes only a very small fraction of the generated power, at such field magnitudes.)

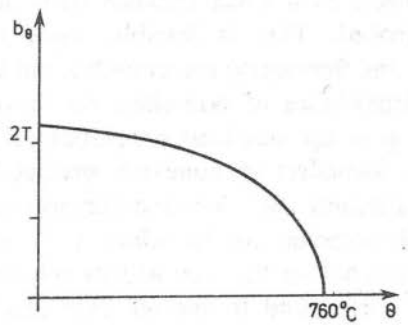

Fig. 3.

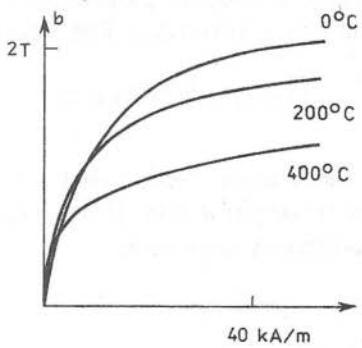

Fig. 4.

The shape of b_θ is quite important; numerical experiments proved this to be one of the two crucial factors which determine the behaviour of the model (the other one is ϱ, dicussed below). On the other hand, results are not sensitive to h_θ, the slope of β at the origin. For this, $h_\theta \simeq 1$ kA/m, modulated in θ according to Ref. (3), was retained. The results are very

close to what a simplified form for β, namely

$$\beta(s) = \mu_0 s + b_\theta \operatorname{sgn}(s) \tag{6}$$

would give. Problem (4) with (5) is Stefan-like. Problem (4) with (6) is the classical Stefan's one. Care was taken so that the numerical methods work equally well on (5) and on (6). Results do not differ significantly. So, though (5) were used in actual simulations, we shall consider the simpler form (6) in the theory.

REMARK. Condition (3) is a simplification. The correct one would be

$$-\varrho \frac{\partial x}{\partial x}(0,t) + l\mu_0 h(0,t) = v(t) \tag{3'}$$

where l is the width of the airgap and v an electromotive force which depends on the electric reaction of the slab on the power alimentation system. Though the software allows to treat (3'), we shall stick to (3) in order to minimize the number of parameters involved in the discussion.

1.1.3. "Thermic" part of the model

To complete the modelling, it remains to state the heat equation, which governs the evolution of temperature θ (q is the enthalpy, k the thermic conductivity)

$$\frac{\partial}{\partial t} q(\theta) - \frac{\partial}{\partial x}\left(k \frac{\partial \theta}{\partial x}\right) = \varrho \left|\frac{\partial h}{\partial x}\right|^2, \quad 0 < x < d, \tag{7}$$

$$k \frac{\partial \theta}{\partial x}(0,t) = 0, \quad k \frac{\partial \theta}{\partial x}(d,t) = 0. \tag{8}$$

The second part of (8) expresses symmetry of θ with respect to the middle plane. The first part means that exchanges of heat by radiation or convection at the edge of the slab are negligible. Indeed, if the airgap is filled with a 10 cm thick refractory material of thermal conductivity 1 W/(m.K), the radiated flux is about 10 kW/m^2 at 1000°C, very small with respect to the injected megawatt per square meter. (Notice nevertheless that, without this protective system, the radiated flux would be around 150 kW/m^2 in the same conditions. As for convection, it can be suppressed with appropriate precautions; but such are unlikeley to be taken in actual plant operations. Experiments at Denain in the North of France around 1978 showed differences of temperature up to 50 degrees, due to this sole factor, between various points of the surface of the slab. Such discrepancies, of course, would ruin the validity of the one-dimensional modelling.)

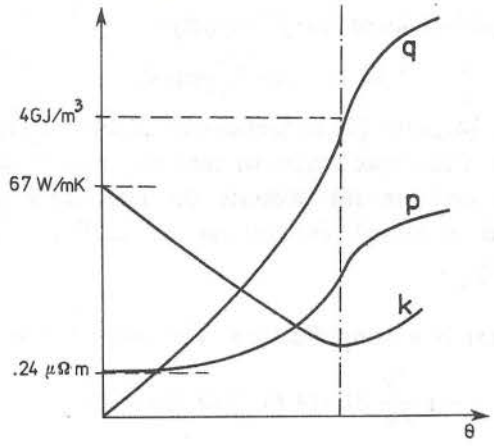

Fig. 5.

Figure 5 shows the behaviour of q, k, and the electrical conductivity ϱ with respect to temperature θ. We call attention to the rapid increase of ϱ with θ.

1.2. Analytical Study

1.2.1. Nature of the coupling

Some dimensional analysis will help understand how (4) and (7) couple together. Let us rewrite the full model, using (6) as constitutive law:

$$\left|\begin{array}{l} \dfrac{\partial}{\partial t}\left(b_\theta \operatorname{sgn}(h)+\mu_0 h\right)-\dfrac{\partial}{\partial x}\left(\varrho_\theta \dfrac{\partial h}{\partial x}\right)=0, \\ h(0,t)=H\sin\omega t,\ \partial h/\partial x\,(d,t)=0, \end{array}\right. \tag{9}$$

$$\left|\begin{array}{l} \dfrac{\partial}{\partial t} q(\theta)-\dfrac{\partial}{\partial x}\left(k\dfrac{\partial\theta}{\partial x}\right)=\varrho\left|\dfrac{\partial h}{\partial x}\right|^2 \\ k\dfrac{\partial\theta}{\partial x}=0 \text{ at } x=0 \text{ and } x=d. \end{array}\right.$$

Let us set

$$\varrho_\theta=\varrho_0\, r(\theta),\ b_\theta=\gamma(\theta)\, b_0$$

where ϱ_0 and b_0 are reference values (those at $\theta=0$), and

$$x=d\xi,\ \tau=\omega t,\ h(x,t)=Hu(\xi,\tau).$$

We get (ignoring a few boundary conditions) a new form of the coupled system:

$$\left|\begin{array}{l} \dfrac{\omega b_0 d^2}{\varrho_0 H}\dfrac{\partial}{\partial\tau}\left(\gamma\,\mathrm{sgn}\,(u)+\dfrac{\mu_0 H}{b_0}u\right)-\dfrac{\partial}{\partial\xi}\left(r\dfrac{\partial u}{\partial\xi}\right)=0 \\ u(0,\tau)=\sin\tau, \\ \tau=\omega t, \\ \dfrac{\partial q}{\partial t}-\dfrac{1}{d^2}\dfrac{\partial}{\partial\xi}\left(k\dfrac{\partial\theta}{\partial\xi}\right)=\dfrac{\varrho_0 H^2}{d^2}r\left|\dfrac{\partial u}{\partial\xi}(\tau)\right|^2 \end{array}\right. \tag{10}$$

which directs attention towards the dimensionless quantities

$$\zeta^{-1}=\mu_0 H/b_0, \quad a=\omega b_0/(d^2\varrho_0 H) \tag{11}$$

(ζ is called the "Stefan's number" of the problem). For typical values like $d=0.05$ m, $\varrho_0=2\,10^{-7}\,\Omega.m$, $b_0=2$ Tesla, $\omega=100\,\pi$, $H=10^5$ A/m, a is of order 1, so in the new unit system, u and $\partial u/\partial\xi$ take on values of similar magnitude, and $\varrho_0 H^2/d^2$ ($\simeq 10^6$ W) is a rough estimate of the volumic Joule power. Knowing that some $Q\simeq 5.\cdot 10^9$ Joule is necessary to get a cubic meter of steel from ordinary to forming temperature, we obtain one hour as an order of magnitude of the overall heating time.

REMARK. By the following computation, based on Cauchy-Schwartz inequality, one gets an upper bound for the heating time. At any time t,

$$|H\sin\omega t|\simeq\left|\int_0^d\frac{\partial h}{\partial x}\right|\leqslant\int_0^d\left|\frac{\partial h}{\partial x}\right|=\int_0^d\frac{1}{\sqrt{\varrho}}\sqrt{\varrho}\left|\frac{\partial h}{\partial x}\right|\leqslant$$

$$\leqslant\left[\int_0^d\frac{1}{\varrho}\right]^{1/2}\cdot\left[\int_0^d\varrho\left|\frac{\partial h}{\partial x}\right|^2\right]^{1/2}.$$

hence

$$\int_0^T dt\int_0^d\varrho\left|\frac{\partial h}{\partial x}\right|^2 dx\geqslant\frac{\varrho_0 H^2}{d}\int_0^T\sin^2\omega t\,dt$$

(since ϱ_0 is a lower bound for ϱ, see Fig. 5), and the left-hand side should be equal to dQ. Therefore,

$$T_{\max}=2Q\frac{d^2}{\varrho_0 H^2}. \tag{12}$$

Though, as we shall see, this is grossly overestimated, it makes apparent the great discrepancy between the time-constants of the two coupled pheno-

mena. Now let us state:

PROPOSITION 1. Let a and ζ be as in (11). If $(u_\varepsilon, q_\varepsilon)$ is solution to the coupled problem

$$\begin{cases} a\dfrac{\partial}{\partial\tau}\left(\gamma_\theta \operatorname{sgn}(u)+\zeta_\theta^{-1} u\right)-\dfrac{\partial}{\partial\xi}\left(r_\theta\dfrac{\partial u}{\partial x}\right)=0,\ 0<\xi<1,\ \tau>0, \\ u(0,\tau)=\sin\tau, \end{cases} \tag{13}$$

$$\begin{cases} t/T_{\max}=\varepsilon\tau, \\ \dfrac{\partial q}{\partial t}\ \dfrac{1}{d^2}\ \dfrac{\partial}{\partial\xi}\left(k\dfrac{\partial\theta}{\partial\xi}\right)=\dfrac{\varrho_0 H^2}{d^2} r\left|\dfrac{\partial u}{\partial\xi}(\tau)\right|^2,\ 0<\xi<1, \end{cases} \tag{14}$$

(plus suitable boundary conditions on θ), then, as ε tends to zero, q_ε tends to q, the solution of

$$\frac{\partial q}{\partial t}-\frac{1}{d^2}\frac{\partial}{\partial\xi}\left(k\frac{\partial\theta}{\partial\xi}\right)=\frac{\varrho_0 H^2}{d^2} f_\theta, \tag{15}$$

where f_θ is obtained by first solving the time-periodic problem

$$\begin{cases} a\dfrac{\partial}{\partial\tau}\left(\gamma_\theta \operatorname{sgn}(u)+\zeta^{-1} u\right)-\dfrac{\partial}{\partial\xi}\left(r_\theta\dfrac{\partial u}{\partial\xi}\right)=0,\ 0<\xi<1,\ 0<\tau<2\pi, \\ u(0,\tau)=\sin\tau,\ \partial u/\partial\xi\,(1,\tau)=0, \\ u(\xi,\tau)=u(\xi,\tau+2\pi),\ 0<\xi<1, \end{cases} \tag{16}$$

then computing

$$f_\theta(\xi)=r_\theta(\xi)\left[\frac{1}{2\pi}\int_0^{2\pi}\left|\frac{\partial u}{\partial\xi}(\xi,s)\right|^2 ds\right]. \tag{17}$$

(All physicists know this result to be correct, and perhaps some mathematician will believe it enough to try and prove it...)

The actual value of ε is here $1/(\omega T_{\max})$, very small as we saw. So, justifiably, one will replace model (13)–(14) — further referred to as "model M_ε" — by (15) (16) (17), "model M_0". This procedure is standard for equations which; like (14), have a rapidly oscillating right hand side, and is known as "averaging".

In the new model, the coupling is a unilateral one. The heat equation has the lead, and the electric equation is subordinate to it. Consequently, we shall now consider the electric equation, assuming a known temperature field.

1.2.2. Linear behaviour (hot steel)

Suppose all temperatures $\theta(\xi, t)$ are above the Curie point. Then, assuming a constant θ for simplicity, the electric equation is

$$\left| \begin{array}{l} \mu_0 \dfrac{\partial h}{\partial t} - \dfrac{\partial^2 h}{\partial x^2} = 0, \ 0 < x < d, \\ h(0, t) = H \sin \omega t, \dfrac{\partial h}{\partial x}(d, t) = 0. \end{array} \right. \tag{18}$$

Periodic solutions to this are found by the well known procedure of complexification. This is easy and tedious, and we refer to [4] for the results. Let us limit ourselves here to the case when d is large. Then,

$$h(x, t) = H \operatorname{Re}\left[\exp\left(-\frac{1+i}{\delta} x + i(\omega t + \pi/2) \right) \right] \tag{19}$$

where δ is the "penetration depth":

$$\delta = (2\varrho/\omega\mu_0)^{1/2} \tag{20}$$

(about 7 cm for steel at 1200°C). The corresponding power profile, once averaged over a time-period, is

$$p(x) = H^2 \frac{\omega\mu_0}{2} \exp(-2x/\delta). \tag{21}$$

Formula (21) describes "skin-effect": the intensity of eddy currents decreases rapidly with depth, and δ is sometimes referred to as the "skin-depth". This is justified by the formula for the impedance of a square meter of heated surface:

$$\mathbf{Z} = (1+i) \frac{\varrho}{\delta} \tag{22}$$

(an easy consequence of (19)) which shows that the Joule dissipation ϱ/δ for a current of efficient value 1 is the same as if eddy currents were evenly distributed in the skin-depth.

The active power, $H^2 \varrho/2\delta$, behaves like $(\varrho\omega)^{1/2}$ for a given H. Thus if one increases the frequency, more power is injected. But this reduces δ, so the power is less uniformly distributed, as (21) shows, and there is a compromise to look for.

1.2.3. Non-linear behaviour ("cold" steel)

Again, let us suppose d is large enough to ignore boundary conditions on the right. Equation (9) with constitutive law (6) becomes (b_θ and $\varrho = \varrho_\theta$

may be assumed constant in time over the period):

$$\begin{cases} \dfrac{\partial}{\partial t}\left(b_\theta \operatorname{sgn}(h)+\mu_0 h\right)-\dfrac{\partial}{\partial x}\left(\varrho \dfrac{\partial h}{\partial x}\right)=0, \ x>0, \\ h(0,t)=H \sin \omega t, \\ h(x,t)=h(x,t+2\pi/\omega)\ \forall t, \ x>0. \end{cases} \tag{23}$$

This is the classical Stefan's problem, but the periodicity condition may confer some new interest to it.

Let us first recall how "moving boundaries" result from (23). In any x interval where h does not vanish, one has

$$\mu_0 \frac{\partial h}{\partial t}-\frac{\partial}{\partial x}\left(\varrho \frac{\partial h}{\partial x}\right)=0, \ x>0. \tag{24}$$

Now let us consider a fixed interval $[x_1, x_2]$ containing (for all t in some time interval) a unique ξ such that $h(\xi(t), t)=0$. Then (Fig. 6), by integrating (23) in x,

$$\frac{d}{dt}\left[\mu_0 \int_{x_1}^{x_2} h(x,t)\,dt+b_\theta\left((x_2-\xi)-(\xi-x_1)\right)\right]- \\ -\varrho \frac{\partial h}{\partial x}\bigg|_{x=x_1}+\varrho \frac{\partial h}{\partial x}\bigg|_{x=x_2}=0$$

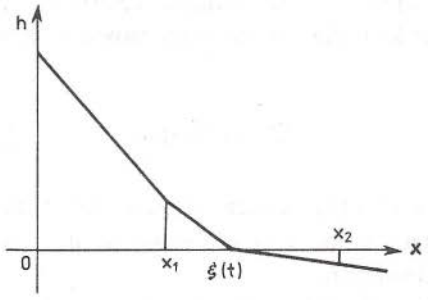

Fig. 6.

thence, by letting x_1 and x_2 tend to $\xi(t)$,

$$2b_\theta \frac{d\xi}{dt}=\left[\varrho \frac{\partial h}{\partial x}\right]_{\xi(t)} \tag{25}$$

($[u]_y$ denotes the jump at point x of a function u). Point $\xi(t)$ is a "moving boundary", or "free boundary", between the two regions characterized by

opposite signs of the induction b or of the field h. Equation (25) relates its speed to the discontinuity of $\partial h/\partial x$ at ξ.

If instead of law (6), we had considered the $b-h$ relation (5), there would be no frank discontinuity of $\partial h/\partial x$, but a rapid change of slope near point $\xi(t)$, where h vanishes. This is the case in the film, but the appearance is that of a moving boundary all the same, for h_θ in (5) is relatively small.

Now, let us proceed to the dimensional analysis of problem (23), by setting

$$\tau = \omega t,\ x = Ly,\ \xi(t) = L\eta(\tau),\ h(x,t) = Hu(y,\tau). \tag{26}$$

Due to the non-linearity, there are now two distinct ways to choose the new unit-length L, depending on the magnitude of the Stefan's number $\zeta = b_\theta/\mu_0 H$. First suppose ζ is small (small b_θ, as when the temperature is just below the Curie point, or large H, say 5 MA/m, something which cannot be achieved with present technology, but could be in the future, with cryogenic devices), and set

$$L = (\varrho/\omega\mu_0)^{1/2} \tag{27}$$

(i.e. $\delta/\sqrt{2}$, δ as defined in (20), but beware ϱ has a different value). This way we get

$$\partial u/\partial\tau - \partial^2 u/\partial y^2 = 0,\quad 2\zeta\, d\eta/d\tau = [\partial u/\partial y]_\eta,\ u(0,\tau) = \sin\tau. \tag{28}$$

When ζ tends to zero, this reduces to the linear case. The "Stefan effect" (presence of well-marked moving boundaries) disappears for very large fields, or when the temperature reaches up the Curie point.

When ζ is large, a more natural choice is

$$L = (\varrho H/\omega b_\theta)^{1/2}\ (\equiv \delta\,(\mu_0 H/2b_\theta)^{1/2}) \tag{29}$$

which yields

$$\frac{1}{\zeta}\frac{\partial u}{\partial\tau} - \frac{\partial^2 u}{\partial y^2} = 0,\ 2d\eta/d\tau = [\partial u/\partial y]_\eta,\ u(0,\tau) = \sin\tau. \tag{30}$$

When $\zeta^{-1} = 0$, (30) can be solved analytically. This has been done in a well-known paper (5). The solution is (Fig. 7):

$$\left|\begin{array}{l} u(y,\tau) = \textbf{if } y < \eta(\tau) \textbf{ then } 2(\eta(\tau) - y)\cos\dfrac{\tau}{2} \textbf{ else } 0 \\[2ex] \eta(\tau) = \sqrt{2}\sin\dfrac{\tau}{2} \end{array}\right. \tag{31}$$

(Remark that, in constrast to what happened in the linear case, this remains correct if the half-width d is finite, provided $d > L$. One just has to complete by symmetry with respect to d.)

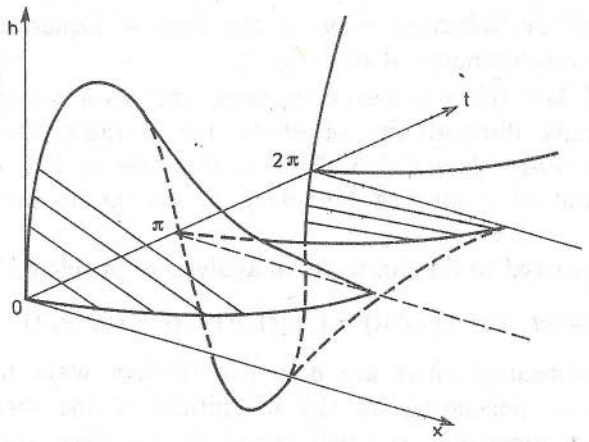

Fig. 7.

From (31), one obtains the average Joule power

$$P = \frac{4}{3\pi} H^{3/2} (2b_\theta \varrho\omega)^{1/2} \tag{32}$$

visualize this later, and see that the distribution is more uniform than in the linear case).

and one could easily plot its distribution along the x-axis. (We shall visualize this later, and see that the distribution is more uniform than in the linear case).

How valid is this limit analysis? A typical value for ζ^{-1} is

$$\zeta^{-1} = \mu_0 H/b_0 = \frac{4\pi\, 10^{-7} \times 10^5}{2} \simeq .06, \tag{33}$$

satisfactorily small. Nevertheless, this is not zero, and one is tempted to look for the next term in some development in ζ^{-1} of the solution. This is not trivial, even for the first order term (see (6)), and there is an interesting problem about the behaviour of the moving boundaries (at steady state, there is an infinity of them), problem which has been presented in (7) and is yet unsolved.

Anyway, as the solution will not depart very much from (31), we may draw qualitative conclusions from the study of this formula:

— Currents are practically confined to a "skin-layer" of depth $L\sqrt{2}$ (the L of (29)).
— This depth depends not only on ω (in $\omega^{-1/2}$), but also on the intensity (in $H^{1/2}$).
— The power is in $H^{3/2}$ (instead of H^2 in the linear case),
— and is more uniformly distributed in the skin-depth.

— Its dependence on ω does not change with respect to the linear case (the power is in $\omega^{1/2}$).

A typical value of the skin-depth is

$$L\sqrt{2} = \sqrt{2}\frac{2\,10^{-7}\times 10^{5}}{100\,\pi\times 2} \simeq 10^{-2}\ \text{m}.$$

If the half-width is 5 cm, this means that eddy-currents are confined to about 20% of the steel, so the effective resistance is much larger than was assumed when we derived the upper bound (12) for the overall heating time, which was thus seriously overestimated.

Plates 1 to 5, made from frames coming from the computer generated movie, show the validity of the conclusions drawn from these analytical studies (Plate 5 corresponds to linear behaviour, Plate 1 to the non-linear one), but also their limitations (Plate 3): the history of the heating process can be summarized as a progressive passage from model (30) (large ζ) to model (28) (vanishing ζ). Nothing else than numerical simulation can tell what happens during the intermediate phase.

2. Numerical methods and results

2.1. Numerical Simulation

2.1.1. The "change of frequency"

The natural way to proceed would be to discretize model M_0, i.e. to solve the leading equation (15) by finite differences and a non-linear Crank-Nicolson scheme, which at each time-step requires one eqaluation of f_θ (and possibly more than one, according to the "predictor-corrector" strategy, which seems the sensible approach here). Computing f_θ would again consist in running a Crank-Nicolson scheme (but with a much more severe non-linearity, when ζ is large). Experience shows that by starting each time from the lastly obtained profile u, and simulating the evolution of u over 5 or 6 half-periods, one gets an acceptable approximation of the periodic solution to (16).

Even so, this amounts to a lot of calculations, and making a movie-necessitates many runs, so we tried to devise something cheaper.

First, modify model M_ε this way. While keeping (13), replace (14) by

$$\frac{\partial q}{\partial t} - \frac{1}{d^2}\frac{\partial}{\partial \xi}\left(\frac{\partial \theta}{\partial \xi}\right) = \frac{\varrho_0 H^2}{d^2}\frac{1}{\pi}\int_{\tau-\pi}^{\tau} r\left|\frac{\partial u}{\partial \xi}(\xi, s)\right|^2 ds \qquad (14')$$

(recall that $t = \varepsilon\tau T_{\max}$). This consists in averaging out the high frequency components of the right-hand side. Let us call M'_ε this modified model.

Now, if M_ε converges to M_0, it is all the more true that M'_ε converges to M_0 (and faster). Ignoring the lack of a suitable proof, we make use of this highly plausible conjecture as follows. The actual value of ε is $1/(\omega T_{\max})$. Instead of replacing ε by 0, multiply it by a large factor α ($\alpha = 155$ in the actual runs), and solve $M'_{\varepsilon\alpha}$ (Fig. 8 should help to get the idea). To

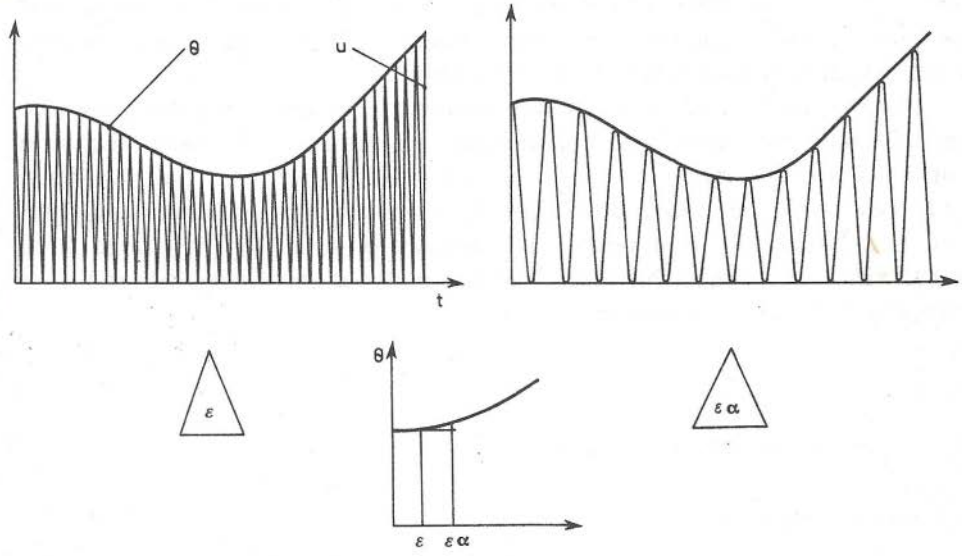

Fig. 8.

summarize, the model that will be discretized and exploited is

$$\left| \begin{array}{l} a\dfrac{\partial}{\partial\tau}\left(\gamma_\theta \operatorname{sgn}(u) + \zeta^{-1} u\right) - \dfrac{\partial}{\partial\xi}\left(r_\theta \dfrac{\partial u}{\partial\xi}\right) = 0,\ 0 < \xi < 1,\ \tau > 0, \\ u(0,\tau) = \sin\tau, \end{array} \right. \tag{34}$$

$$\omega t = \alpha\tau, \tag{35}$$

$$\frac{\partial q}{\partial t} - \frac{1}{d^2}\frac{\partial}{\partial\xi}\left(k\frac{\partial\theta}{\partial\xi}\right) = \frac{\varrho_0 H^2}{d^2}\frac{1}{\pi}\int_{\tau-\pi}^{\tau} r_\theta \left|\frac{\partial u}{\partial\xi}(\xi, s)\right|^2 ds. \tag{36}$$

Thanks to the multiplicative factor α, the ratio of the time constants of (36) and (34) is reduced in proportion, so it now becomes feasible to solve (34) (36) as a coupled evolution problem. The scheme will be a Crank-Nicolson one for (36) and an explicit one for (34), and the great commodity of taking the same time step for both is allowed, for the stability condition is satisfied

by a large margin. The non-linear system in u which has to be solved at each time step is treated by a variant of SSOR (quite alike Elliott's scheme as published in (8)).

This approach is cheaper than the previous one by a factor of 10. The toll to pay in accuracy is not too heavy, if one can interpret in this way the observed stability of results with respect to α (runs with $\alpha = 150$ and $\alpha = 300$ match up to the second decimal place).

2.1.2. Making the movie

Each frame shows two graphs (see Plate 1): the field h above, the power profile below. The temperature is only indicated by a white mark showing the abscissa of the point at 760°C. These dispositions, which have been adopted after a series of trials and errors, are justified as follows.

The idea was to make all phenomena simultaneously visible. This obviously supposes some distorsion of time scales, since there is a fast dynamic and a slow one. The compression ratio already introduced by the "change of frequency" method is thus welcome, but not sufficient. As the apparent speed of a moving curve in the viewing window cannot be too large, the apparent period of the magnetic field should be, for visual comfort, at least 5 seconds. The complete run would make, at this rate, a movie of about 20 minutes (more or less the actual duration of the heating process), hardly bearable. We thus set H to the high (and a bit unrealistic) value of $7\,10^5$ A/m. The overall sequence then lasts about 2 minutes (and non-linear effects are enhanced, which is for the best).

Even so, it was not felt necessary to display the graph of the instantaneous temperature. Indeed, the heat diffusion is governed by a Stefan's model, and one would like to see the corresponding free boundary (i.e. the point x at 760°C) as it moves. But the Stefan's number (ratio of the phase-transition latent heat to the total enthalpy Q) is small, and the diffusivity relatively high, for a width of the slab of 10 cm. All these reasons concur to produce nicely smooth temperature profiles whose evolution, devoid of any noticeable Stefan effect, would make a very dull show. It was enough to point at the position of the 760°C abscissa. The pointer is the small black square which appears first in Plate 3, signalling that the zone to its left is above the Curie point.

The mean power density, which appears as vertical stripes at the bottom of the frame, completes the information about the thermic phenomenon.

By looking at the graph in x of $h(x, t)$, one could in principle visualize the instantaneous power density $\varrho\,|\partial h/\partial x|^2$ as a function of x, which is also interesting information. It was soon realized that such visualization was beyond the capacities of our eye-plus-brain system. So two identical runs are shown in succession in the final movie. One displays the mean value

of the power over the time period (Plate 6 is made from selected frames out of this sequence). The other one shows the instantaneous power profile.

The graphic conventions are the less unsatisfactory we could select, after many attempts. It is amazingly easy to hinder the right perception of phenomena by a poor choice of such conventions, and ours certainly leave room for improvement. For instance, it would have been better to display all curves on the full interval $[0, 2d]$, notwithstanding symmetry, instead of on the left half $[0, d]$.

Lots of nagging problems (which tend to be left unperceived when one relies on static graphic renderings) were encountered. Two of these might be of interest from the point of view of the numerical analyst. When solving a Stefan problem on a fixed grid, especially a rather coarse one like ours (40 nodes), one can observe weak instabilities due to the dicontinuous movement of the free boundary, which jumps from node to node. This affects the slope of the computed profile as explained in Fig. 9. This flip-flop

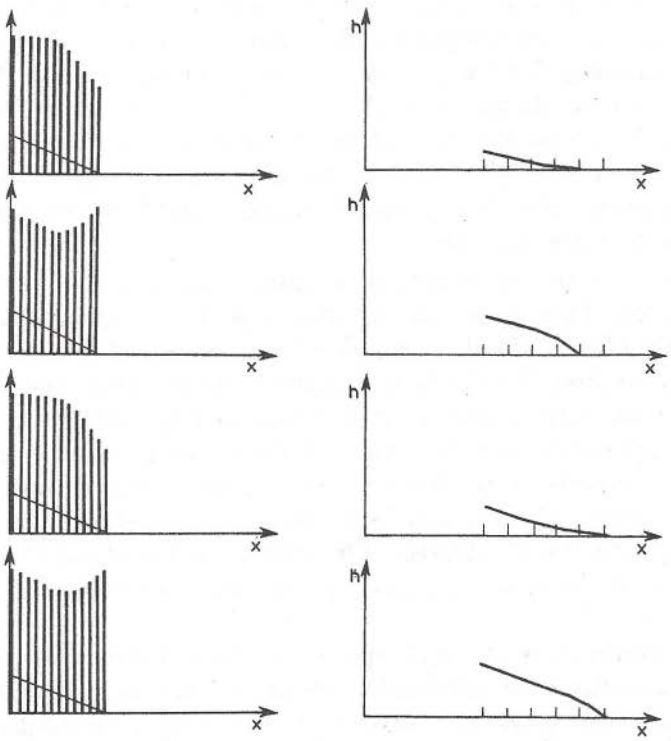

Fig. 9. The "flip-flop" effect. On the left, four successive profiles of the power $\varrho\,|\partial h/\partial x|^2$. The thin line is the graph of h. On the left, h again, but the instability is exaggerated to suggest the origin of the flickering effect

effect, hardly noticeable on successive static graphs, is amplified by numerical differentiation, and results in a disastrous quivering of the instantaneous power profile. There is also a great sensitivity of the computed free boundary to the stopping criterion in the non-linear overrelaxation algorithm. If this is not carefully adjusted, the free boundary (as considered in the $x-t$ plane) is jagged, which results in random jerks of the h-profile as seen on the screen.

There are simple remedies to all these defects, and all things considered, the combination of non-linear SSOR and Crank-Nicolson scheme proves to be a cheap and robust approach, which works well on a wide range of values of the Stefan's number, and for all shapes of the non-linear characteristics. Its extension to dimension 2 also proved satisfactory.

2.2. Results

The precise values of the parameters were: $H = 7 \cdot 10^5$ A/m, $d = .056$ m, $\omega = 100\,\pi\,(50\,Hz)$, α (the frequency ratio) $= 155$. The $b-h$ relation was (5) with $h_0 = 10^3$ A/m. Other characteristics are as in Figs. 4 and 5. There are 40 nodes in the finite difference grid (the same for both dynamics), and 60 time-steps in a half-period. Sensitivity to various parameters was tested, and it is felt that all quantities of physical interest are computed to within 2% accuracy, at the worst.

Plates 1 to 4 are all similarly made by taking one frame out of 16 over a period of time which corresponds to approximately one and a half full period of the electric excitation. This way, each Plate consists of 24 frames, arranged columnwise (first frame at top left, next one below, etc.) Each sequence begins at approximately the time when $h(0, t) = 0$, going up. So one can follow the free boundary, created at this instant at $x = 0$, and moving right. Every time $h(0, t)$ passes zero, a new free boundary is thus created, and starts chasing after the last one. Some frames show as many as three such boundaries. They die when they reach the position $x = d$, where they meet their mate, coming from the right side of the slab (and not represented in our frames). Their life span is such that about thirty of them should be present at certain moments (Plate 3), but they all accumulate at the bottom of the skin-layer, where they cannot any more be individualized by the numerical scheme.

What is shown at the bottom of each frame is the instantaneous power profile. The succession of time-averaged profiles is displayed in Plate 6.

Plate 1 corresponds to the transient behaviour at the beginning of the simulation. During this phase, the thermic characterictics of the steel do not change, for the temperature is not allowed to grow until a satisfactory steady-state (periodic solution of (16)) is attained. This phase lasts 2 periods. Then the temperature starts growing. In this phase, the penetration depth

is about one half of the x-interval (which itself corresponds to the half of the slab). What should be noticed is the very sharp distinction between the zone concerned by eddy-currents and the "dead-core" on the right, where nothing happens. This is characteristics of non-linear behaviour (Stefan effect). The notion of "penetration depth" is thus a very tangible one, much more so than in the linear case, where it is just a convention. What the first Plates thus show is "non-linear skin-effect".

Next plate (#2) shows the state of affairs when the steel has been heated for a while. Its resistivity is now higher, and parameter b_θ (the so-called "saturation induction") is smaller. According to formulas (29) and (31), the penetration depth has increased. Let us now suggest a more refined analysis than the one we did in §1.2.3, which consists in allowing L to vary with x in the changes of units (26): L is given by (29), but ϱ and b_θ take on at point x the values coresponding to the temperature at this point. As the temperature falls from left to right, L similarly decreases. From a computation similar to the one which led to (31), one obtains the power profile and finds that, because of this decrease in L, the profile tends to develop a "hump" on the right side, just at the left of the free boundary. This phenomenon can be observed on Plates 2 and 3. It is thus due to the increase of ϱ and the decrease of b_θ with temperature. This phenomenon is favourable, from the point of view of the efficiency of induction heating, since it favours a more uniform repartition of Joule power.

Next plate (# 3) corresponds to the time when the Curie point has just been overtaken in the material beneath the surface of the slab. Notice how the power profile neatly suggests two different behaviours: linear on the left, non-linear on the right. The penetration depth continues to increase. One may interpret phenomena correctly by imagining a composite of two different materials, one with linear behaviour, the other, non-linear, flanking it. The black dot indicates the boundary between them.

Now a new phenomenon appears. Up to now, two new free boundaries were created at each time-period, and would go to the right while losing their velocity. Now, all old free-boundaries have at last reached $x = d$, where they met their mirror image, and vanished. A new steady state is now reached, where moving boundaries only last a fraction of the half-period, and impinge on their right-side homolog at finite speed. This is clearly shown by Plate 4. Notice also that they are no more born at $x = 0$, but at some point slightly below the Curie temperature (this phenomenon is much easier to see dynamically than on static frames). The hotter the steel, the shorter the life of free boundaries, and the narrower the interval of their course. Eventually (Plate 5) they disppear completely, and the linear regime prevails in the whole width of the slab.

There is an important consequence. During this time interval between the death of a moving boundary and the birth of the next one, the regime

is linear (no value of x such that $h(x,t)=0$, so Eq. (24) is valid). But the value of ϱ is now such (see Fig. 5) that the penetration depth (20) is greater than the half-width. This results in a small resistance of the slab, and consequently the injected power drops to very small values. In other words, induction heating is effective only during this part of the period of the driving current when moving boundaries are present. We thus have here an example of an engineering problem where free boundaries are welcome, and an essential feature of the process.

Figure 10 shows the evolution of the active power.

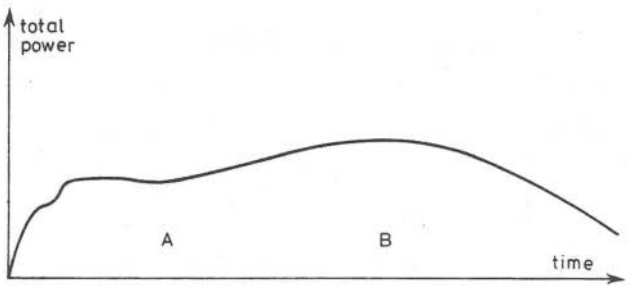

Fig. 10. Power (averaged over a time period) as a function of time. The left part corresponds to the computation of the steady state at initial temperature: after a numerical transient, the power settles at its initial value. Heating starts at date A. The maximum of power (point B) corresponds to the time when the side of the slab attains 760°C

The repetition of all what precedes in two dimensions would also be of interest, for it corresponds to the problem of heating "long products", like threads and billets. No new qualitative features emerge, in fact. Plate 7 shows the profile of field h, as function now of two space variables x and y in a half-section of a billet, and over a time-period. The "dead-core" phenomenon is obvious.

Conclusion

We have presented a model of a situation of industrial interest where moving boundaries play a key-role. The model lends itself to some analysis which points to the importance of free boundaries as regards the very efficiency of the process, and to a numerical treatment which reveals new aspects of the behaviour of the model, and gives new evidence in the same direction. A simple rule emerges: an optimal heating process would be obtained if the moving boundaries could be controlled in such a way that they be always present and run across the whole portion of space available, or nearly so. More precisely, making use of the concept of penetration depth,

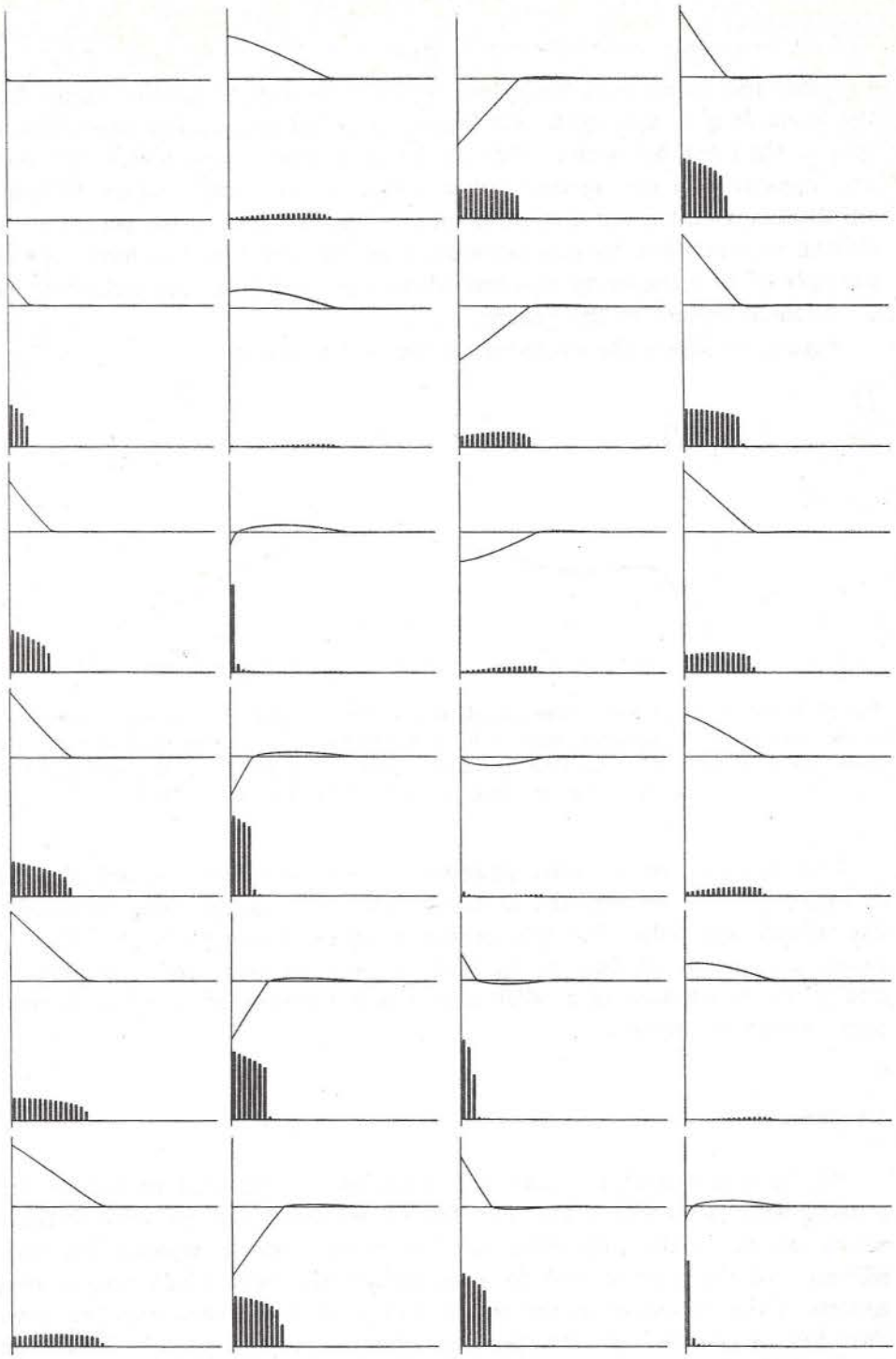

Plate 1. Beginning of the simulation. The temperature is not yet allowed to vary, not before the magnetic steady-state has been established. Each frame shows two graphs over the same x-interval: field (top) and instantaneous power (bottom). A full period of the driving current corresponds to 16 frames

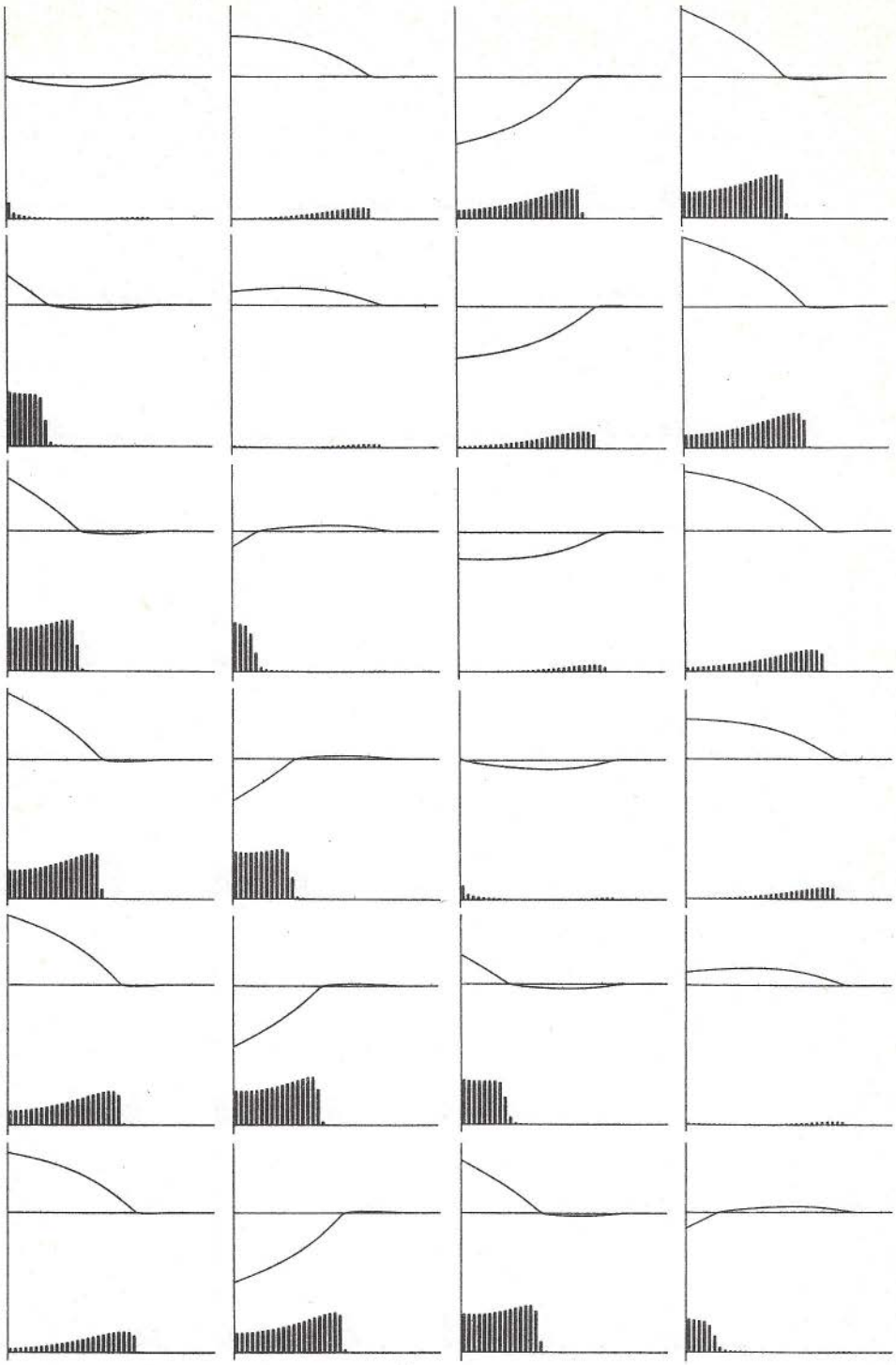

Plate 2. After some heating. The depth has increased. Non uniformity of the temperature (which explains the "hump" of the power profile)

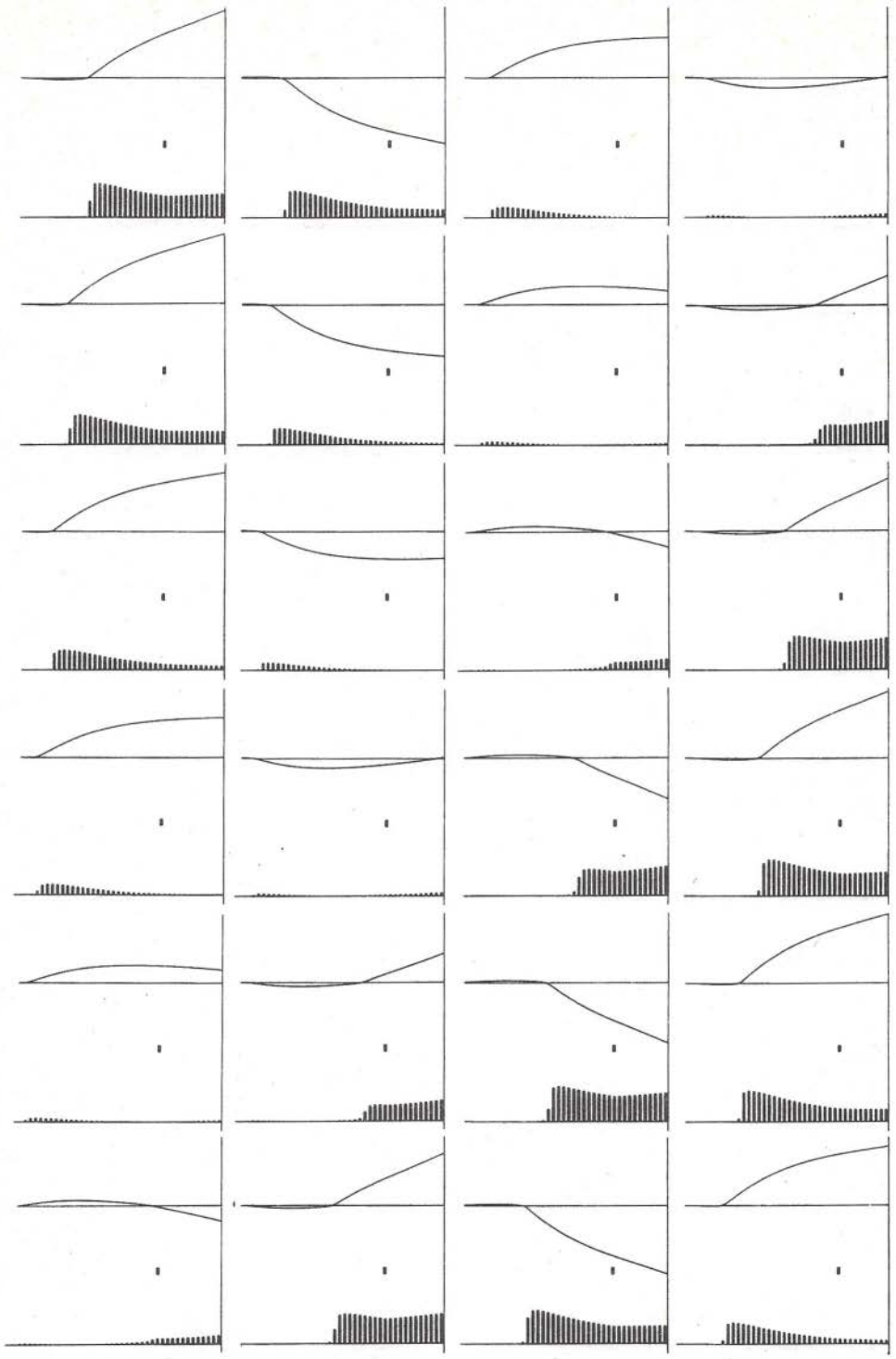

Plate 3. Surface has just crossed the Curie point (760°C, the black dot points to the abscissa at 760°C). Coexistence of "linear regime" (left to the dot) and "non-linear regime" (right)

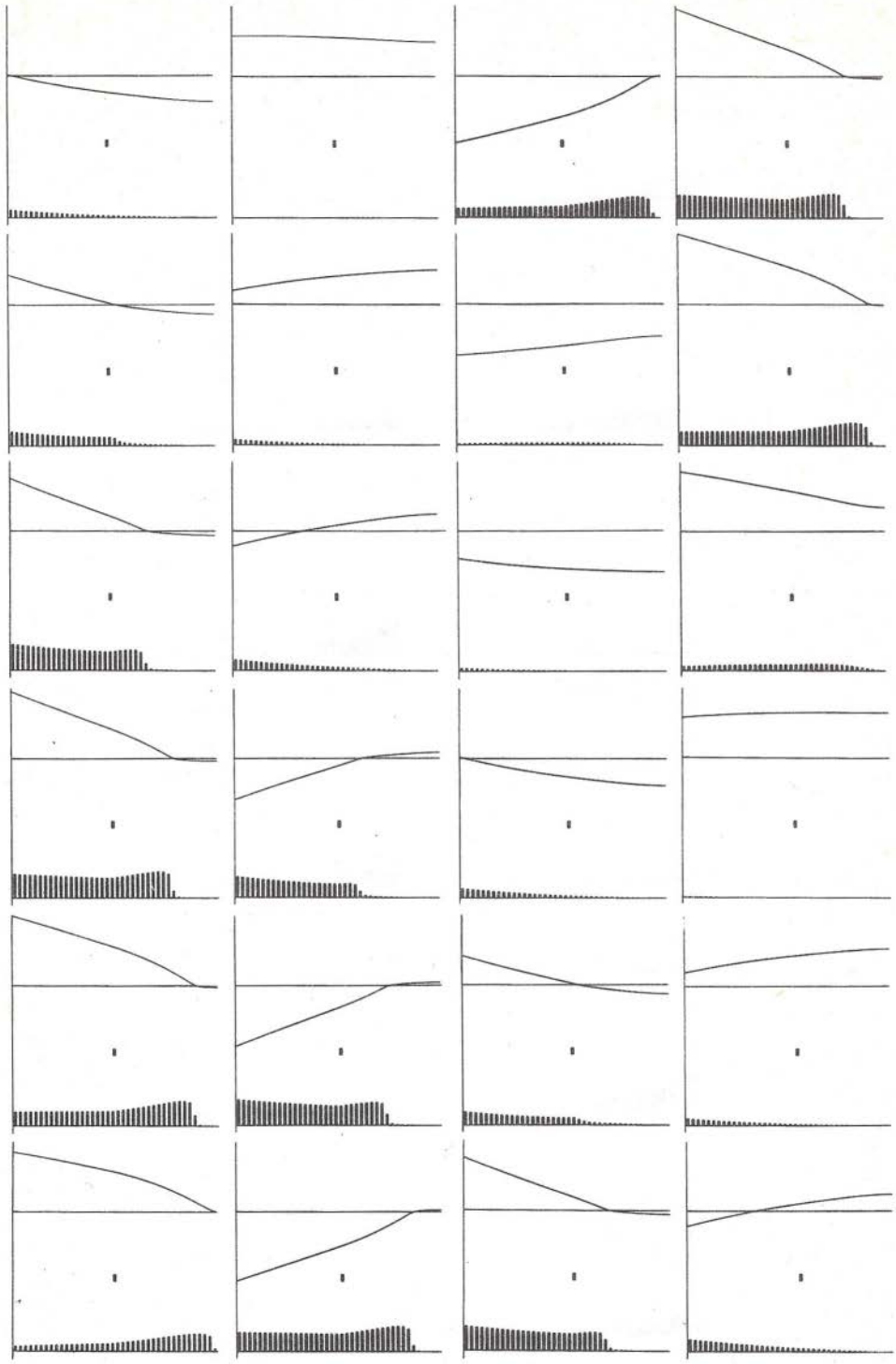

Plate 4. New phase, where free boundaries will disappear during a fraction of each time-period (frames 7–9, 14–16)

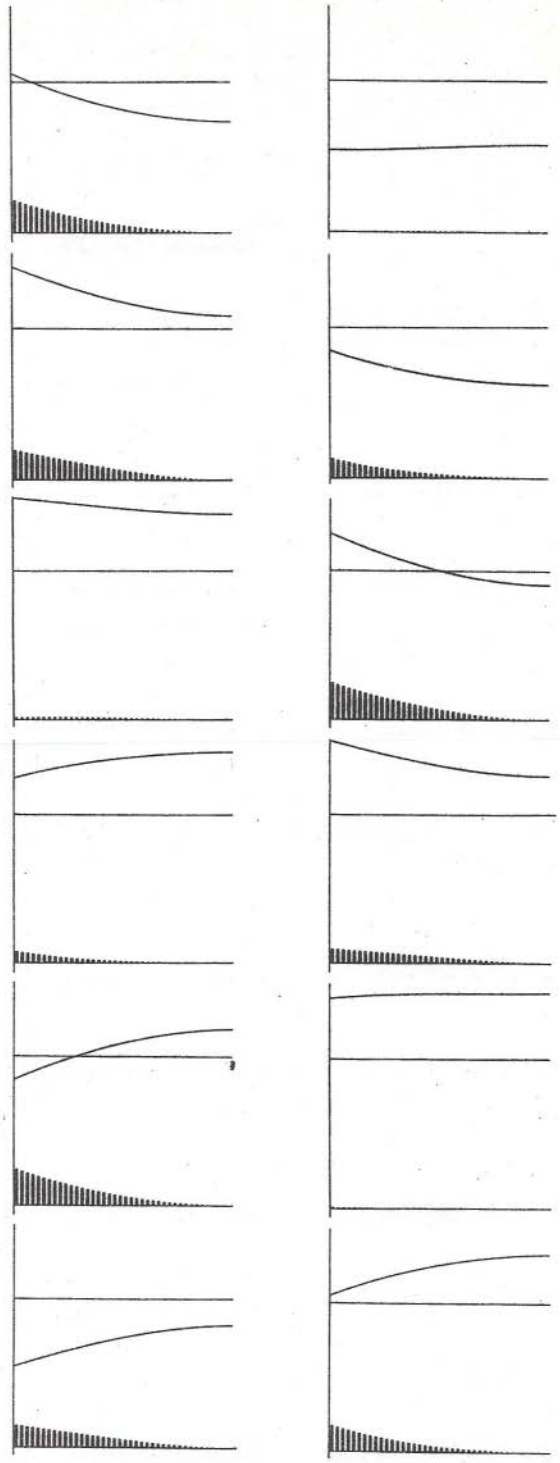

Plate 5. All points largely above Curie temperature. Linear regime. The penetration depth is greater then the half-width. (In this run, the frequency were doubled during this phase: 8 frames for a full period.)

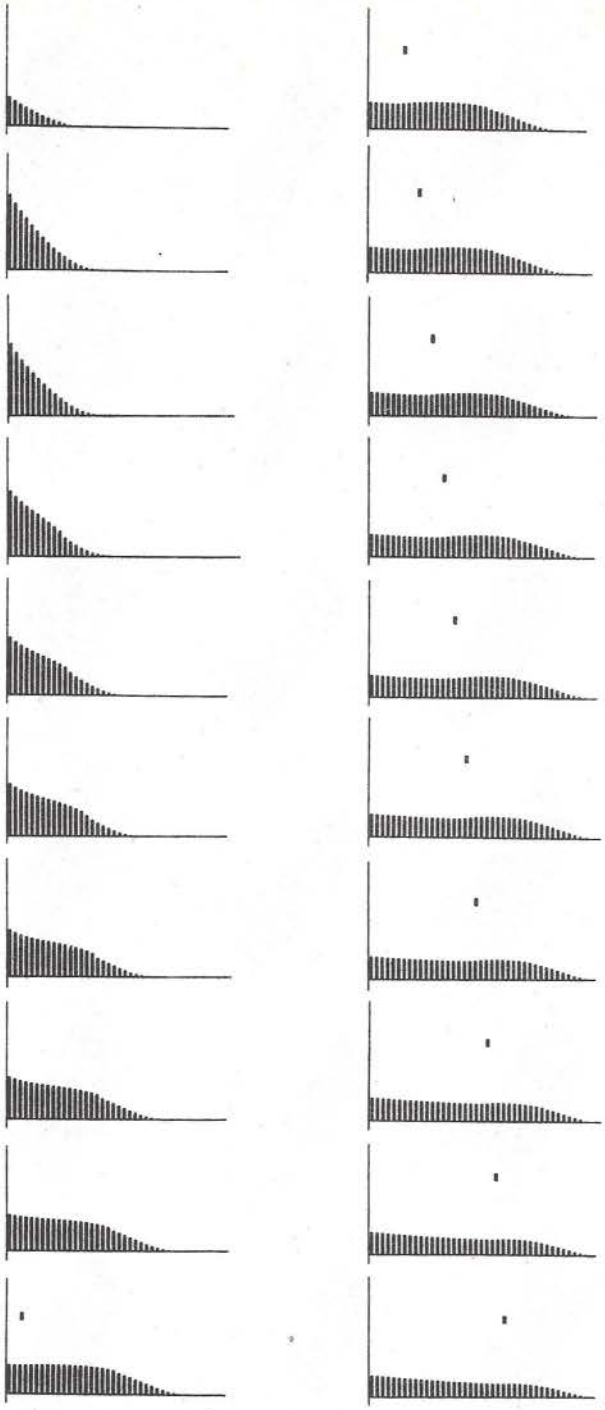

Plate 6. Time-averaged power profile during the simulation. Heating begins at frame 4. For the total power as a function of time (surface of the shaded area) see Fig. 10

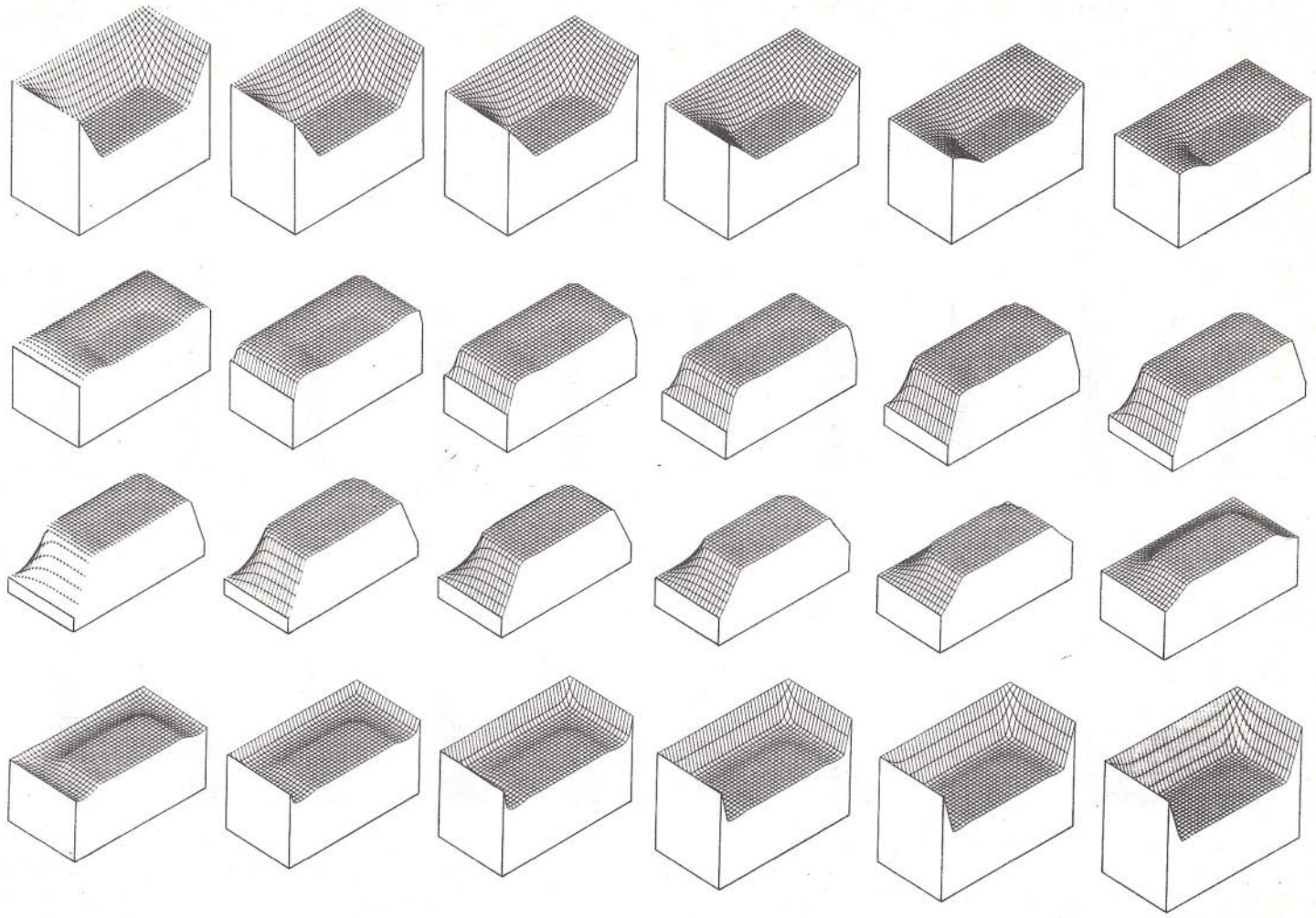

Plate 7. A 2-D simulation, in similar conditions. A "dead-core" effect is clearly visible. (Each frame shows h in terms of the two space variables, at a given time.)

this depth should always be slightly below the half-width of the slab, in the case we studied. A similar rule seems to hold for other shapes of heated workpieces.

Now, two main controllable parameters influence the penetration depth, as shown in §1.2.3: The frequency ω and the peak value H of the magnetic field in the airgap. Suppose one wants to inject a total power p and to distribute it over a depth λ as equally as possible. According to formulas (29) and (32), and assuming the Stefan's number is large, one should take

$$\omega = \frac{1}{\lambda b_0} (\varrho p)^{1/2} \left(\frac{3\pi}{2}\right)^{1/2}, H = \lambda (p/\varrho)^{1/2} \left(\frac{3\pi}{8}\right)^{1/2} \tag{37}$$

as a starting point. Corrective multiplicative factors may have to be put in, but (37) shows the control strategy at the beginning of the heating cycle (the most important phase): ω should grow like $\sqrt{\varrho_\theta}/b_\theta$, and H should decrease like $\varrho_\theta^{-1/2}$. After this, no simple formula exists, but the implementation of the same strategy through a numerical scheme is obvious and simple.

References

[1] BOSSAVIT A., DAMLAMIAN A., FRÉMOND M. (Eds.) Free boundary problems: applications and theory. Vols. III and IV, Boston, Pitman, 1985.

[2] FASANO A., PRIMICERIO M. (Eds.) Free boundary problems: theory and applications. Vols. I and II, Boston, Pitman, 1983.

[3] ROSS N. V. A System for Induction Heating of Large Steel Slabs. *IEEE Trans. IGA*, **5**, Sept., Oct., 1970.

[4] BOSSAVIT A. Impédance d'un four linéaire à induction, in: Proc. World Electrotechnical Congress (June 21–25, 1977), Sect. 4A, Rpt. No. 45.

[5] AGARWAL P. D. Eddy-current Losses in Solid and Laminated Iron. *AIEE Trans. on Comm. and Electronics*, **78**, Pt. II (1959), 169–79.

[6] BOSSAVIT A. Numerical Determination of an Equivalent Complex Permeability for Saturated Steel, in: Proc. "Compumag" Conference on the Computation of Magnetic Fields, Oxford, 31–2 April 1976 (Rutherford Laboratory, Oxon OX11 OQX, U.K.), 282–86.

[7] BOSSAVIT A. in Ref. (2), pp. 349–64.

[8] ELLIOTT C. M. On the Finite Element Approximation of an Elliptic Variational Inequality Arising from an Implicit Time Discretization of the Stefan Problem. *IMA J. Numer. Anal.*, **1** (1981), 115–125.

Swobodne granice w grzaniu indukcyjnym

Praca omawia szereg eksperymentów numerycznych symulacji procesu grzania indukcyjnego bloków stalowych. Proces ten będący przykładem interesujących swobodnych granic stawia liczne pytania natury teoretycznej. Sama obecność ruchomych granic wiąże się z efektywnością grzania, prowadząc do zagadnień sterowania, które leżą u podstaw przedstawianej pracy. Wyniki eksperymentów symulacyjnych zostały przedstawione w formie graficznej jako komputerowo wygenerowany film.

Свободные границы в индукционном грении

Работа оговаривает ряд численных экспериментов симмуляции индукционного грения сталевых слабов. В процессах такого рода образуются. интересные свободные границы, принося многие теоретические вопросы. Уже само существование движущихся границ связанно с эффективностью грения, отсюда возникают проблемы управления, основоположны для предлагаемой работы. Результаты иммитационных экспериментов представлены графически в виде компютер-фильма.